Study of the Effect of Siliceous Species in the Formation of a Geopolymer Binder: Understanding the Reaction Mechanisms among the Binder, Wood, and Earth Brick.

Fabrice Gouny, Fazia Fouchal, Pascal Maillard, S. Rossignol

I&EC research
Industrial & Engineering Chemistry Research

Article

pubs.acs.org/IECR

Study of the Effect of Siliceous Species in the Formation of a Geopolymer Binder: Understanding the Reaction Mechanisms among the Binder, Wood, and Earth Brick

Fabrice Gouny,[†,§] Fazia Fouchal,[‡] Pascal Maillard,[§] and Sylvie Rossignol*[,†]

[†]Groupe d'Etude des Materiaux Heterogenes (GEMH-MMGD), Ecole Nationale Superieure de Ceramique Industrielle, 12 rue Atlantis, 87068 Limoges, France

[‡]Groupe d'Etude des Materiaux Heterogenes (GEMH-GCD), Boulevard Jacques Derche, 19300 Egletons, France

[§]Research and Development Department, Centre Technique de Materiaux Naturels de Construction (CTMNC), Ester Technopole BP 26929, 87069 Limoges Cedex, France

* Supporting Information

ABSTRACT: In building construction, geopolymer binder or mortar can interact with the structural materials and thus modify the binder formation mechanisms. In a geopolymer binder, the availability and amount of siliceous species is a preponderant parameter influencing the nature of networks formed after consolidation. In this study, the interactions between the binder and structural materials (wood and earth bricks) were investigated by ^{29}Si magic angle spinning nuclear magnetic resonance (MAS NMR) and Fourier transform infrared spectroscopy (FTIR) during and after the consolidation. Then, the effect of the amount and nature of the siliceous species available in the reaction medium were analyzed. According to the siliceous species available, it is possible to form different types of materials (hardening or sedimented materials). By corroborating these results with MAS NMR and FTIR analyses, a formation scheme of the binder in contact with the materials was proposed.

INTRODUCTION

Currently, the reduction of CO_2 emissions has become a global concern, and the investigation of environmentally friendly materials has become increasingly important.[1−3] In this context, the use of natural materials, such as the wood and earth materials that have been used for several millennia, seems to be relevant.[4−6] Earth materials (i.e., unfired clay bricks or rammed earth) offer many advantages, including a weak embodied energy, the ability to regulate the relative humidity of a building as a result of their hygroscopic properties, their abundance in most areas, and ease of recycling.[5,7] Indeed, by using local materials, the environmental impact of the construction is drastically reduced as well as the price of the final product.[8] Moreover, Allinson and Hall[9] have shown that earth walls can buffer relative humidity changes in a room by adsorbing moisture in a high humidity period and releasing it later, which improves the hygrothermal comfort of the building. The wood, from its mechanical characteristics, brings lightness to the structure. Timber frame construction with earth brick infill appears today as a sustainable design that is promising in the building construction field. However, cracks form at the interfaces of the bricks and frame with temperature and humidity fluctuations because of shrinkage and swelling phenomena (with wood and earth being hygroscopic). Research on new binders with the ability to adhere to wood, especially on earth bricks, has thus been performed.[10] Among the potential materials currently available, the geopolymer type is a potentially good candidate. For example, a recent study showed that the addition of silica fume to a geopolymer mixture leads to the formation of a foam that has the ability to adhere to wood.[11] Moreover, previous works on construction designs made from wood, earth bricks, and these geomaterial foams have indicated the viability of these structures by demonstrating the ability of the geopolymer binder to produce strong bonds between the wood and earth.[12,13] Mechanical shear tests on these masonry have shown that their shear strength values range from 1.5 to 2 MPa, depending on the type of brick.[12] Furthermore, from the results and observations of pull-out tests, the adhesion mechanism was principally explained by mechanical interlocking.[13] In the case of binder−brick adhesion, it has been shown that there is first absorption of the binder by the pore of the brick and then chemical interactions with the creation of an interphase.[13] In the case of binder−wood adhesion, anchor points were also created by the penetration of the binder inside the pore of the wood before the binder consolidation. This observation was justified by an X-ray map of the element potassium realized on the wood/binder interphase.[12] Next, the effect of the penetration of the binder inside the materials and the consequences on the binder formation must be understood. Specifically, if the binder penetrates the materials, it induces chemical interactions that could modify the reaction mechanisms during the consolidation. Investigation of the nature of the networks formed after consolidation and contact with the materials is thus necessary.

Geopolymers are amorphous three-dimensional aluminosilicate binder materials that are synthesized at ambient temperature by the alkaline activation of aluminosilicate sources, such

Received: October 30, 2013
Revised: January 27, 2014
Accepted: February 10, 2014
Published: February 10, 2014

   dx.doi.org/10.1021/ie403670c | Ind. Eng. Chem. Res. 2014, 53, 3559−3569

as calcined clays, industrial waste, and more.[14,15] These materials show good resistance to high temperatures and acid degradation, as well as good compressive strength. Their formation results from the dissolution and reorganization of raw materials. First, reactive aluminosilicate sources are dissolved to form free $Si(OH)_4$ and $Al(OH)_3$ species, which will then react by a polycondensation reaction to form an amorphous geopolymer network. To further understand and highlight the different network formations, atomic bond scale analyses (Si−O−M, M = Si, K, Al) are necessary. Magic angle spinning nuclear magnetic resonance (MAS NMR) analysis is a useful characterization technique for investigating the silicon environment in the binder. This technique allows the determination of the different networks that can be formed in the binder after contact and consolidation with the natural materials.[29]Si MAS NMR analysis, conducted by Autef et al. on geopolymer materials, has highlighted different contributions that correspond to different silicon environments.[16] These results showed five contributions centered around −80, −88, −97, −106, and −113 ppm, which are attributed to $Q^3(2Al)$, $Q^4(3Al)$, $Q^4(2Al)$, $Q^4(1Al)$, and $Q^4(0Al)$ from silicic acid bonds, respectively (more details in the Results). In situ Fourier transform infrared spectroscopy (FTIR) is another widely used technique for the study of the formation of the polymer network.[17] It is particularly efficient for following the structural evolution of materials in the polymerization process, notably, the substitution of Si−O−Si by Si−O−Al bonds, which is characteristic of the geopolymerization reaction.[18]

This work thus completes previous works on the use of a geopolymer binder in timber-framed construction using earth bricks as in ll. This study attempts to understand the reaction mechanisms intervening between the natural geopolymeric binder and natural materials (wood and earth brick) and proposes a formation model of the binder in the function of materials in contact. First, the results of in situ FTIR and ^{29}Si MAS NMR analyses performed on the binder, which was consolidated in contact with materials, are presented. Next, 30 geopolymer binder formulations were investigated by in situ ATR (attenuated total reflection) FTIR analysis, which should allow a better understanding of the effect of the siliceous species on the nature of the formed networks.

MATERIALS AND METHODS

Raw Materials. In this study, several precursors and raw materials were used with distinguished precursors for the binder synthesis and raw materials used for the building system (earth brick and wood). Concerning the mineral polymer binder, various samples were synthesized using potassium hydroxide pellets (85.7% purity), potassium silicate solution (H_2O = 76.07%, SiO_2 = 16.37%, and K_2O = 7.56%), metakaolin M1000 from AGS (Clerac, France), and silica fume. Three types of silica were used: silica fume supplied by Feropem (denoted FDS), silica fume supplied by Cabot (denoted M5), and crushed quartz (denoted Si400). Details of all silica used in this work are presented as Supporting Information (Table S1).

Concerning materials applied for the building system, two extrusion-manufactured industrial earth bricks were chosen, the same bricks used in previous work.[12,13] The bricks differed in mineral composition (denoted Br_1 and Br_2), and their densities were 1.70 and 2.00 g cm^{-3} for Br_1 and Br_2, respectively. A local company of Limoges, France, supplied Douglas fir wood that was dried and planed. The details of assembly manufacturing are presented in previous work.[12,13]

Sample Preparation. All binders were prepared by magnetic stirring of the potassium hydroxide pellets in the solution of potassium silicate, followed by the addition of the silica fume (or quartz) and metakaolin. It is important to distinguish that the reference FDS_{100} binder is used for the final composite system and the other binders were used to investigate the effect of silica on the nature of the networks formed during the consolidation of the material. Figure 1 summarizes the synthesis protocol of foam FDS_{100} and other binders.

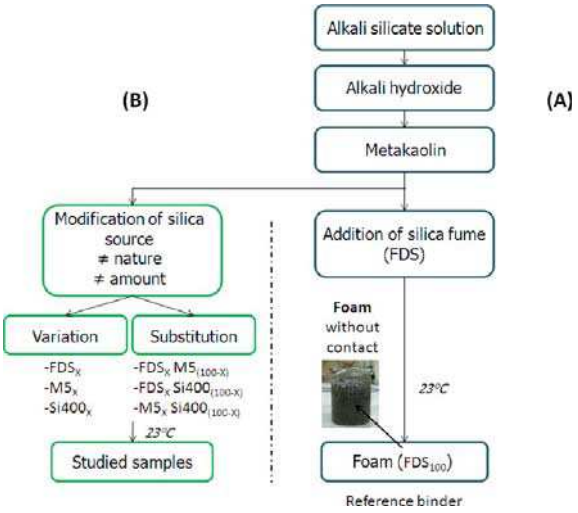

Figure 1. Synthesis protocol of geomaterial foam (A) and other samples synthesized based on foam formulation (B).

The type and amount of silica introduced into the mixture directly influence the characteristics of the final binder. To assess their influence, two binder series have been developed, which are noted as substitution (FDS_XM5_{100-X}; FDS_XSi400_{100-X}; $M5_XSi400_{100-X}$) and variation (FDS_X, $M5_X$, $Si400_X$). For each series of binder, the amount of metakaolin, potassium silicate, and potassium hydroxide remain identical, as for the reference foam FDS_{100}; only the type and the amount of silica added to the mixture have been modified. Nomenclature examples for the synthesized binders are presented as Supporting Information (Table S2). The indexed number between 0 and 100, which appears after the name of the used silica, is the weight percent of the silica introduced into the mixture. The substitution samples have the same weight percent of silica as the reference FDS_{100}; only the type of each silica introduced changes. For variation samples, the weight percent of introduced silica varies from 0 to 100% in 20% increments. Shown on Si−Al−K−O ternary, it is noted that synthesized binders correspond to sedimentary materials and gels according to the work of Gao et al.,[19] as shown in Figure 2.

To evaluate the effect of the contact of the structural materials (earth bricks and wood) on the consolidation and network formation of the reference binder FDS_{100}, the binder in contact with these materials was analyzed. For this experiment, a hole was drilled in the materials, and the reference binder (foam FDS_{100}) was poured inside. In situ FTIR analysis was performed during consolidation and MAS NMR analysis after consolidation.

Characterization Techniques. FTIR spectra were obtained using a Thermo Scientific Nicolet 380 infrared

dx.doi.org/10.1021/ie403670c | Ind. Eng. Chem. Res. 2014, 53, 3559−3569

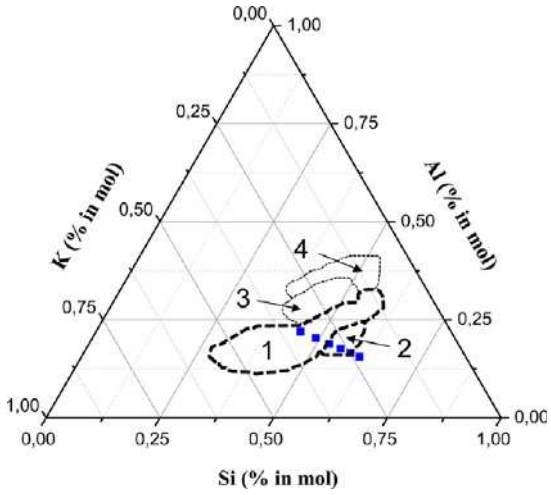

Figure 2. Blue squares show the position of mixtures synthesized on the (Si−Al−K−O) ternary (existence domains of several mixtures proposed by Gao et al.: 1, sedimented materials; 2, gel; 3, geopolymer; and 4, hardening materials).

spectrometer using the ATR method. The IR spectra were collected between 500 and 4000 cm^{-1}, with a resolution of 4 cm^{-1}. To monitor sample formation, a macro was used that allowed spectra to be recorded every 10 min for 10 h. The acquisition was initiated after placing a drop of sample, or the material with binder inside, onto a diamond substrate. Finally, overlaid raw spectra were obtained. To remove the contribution from atmospheric CO_2, the spectra were corrected with a straight line between 2280 and 2400 cm^{-1}. The spectra were corrected using a baseline and then normalized before being compared.

High-resolution MAS NMR experiments were performed at room temperature in a Bruker AVANCE-400 spectrometer operated at 79.49 MHz (^{29}Si signal). The ^{29}Si ($I = {}^1/_2$) MAS NMR spectra were recorded after $\pi/2$-pulse irradiation (4 μs) using a 500-kHz filter to improve the signal/noise ratio. In the MAS NMR experiments, powder samples were spun at 10 kHz. The number of scans was 400 for silicon. The time between accumulations was set at 10 s to minimize saturation effects. Spectral deconvolution was performed using the Wint (Bruker) software package. The deconvoluted spectra are only used qualitatively, and no quantitative studies have been performed.

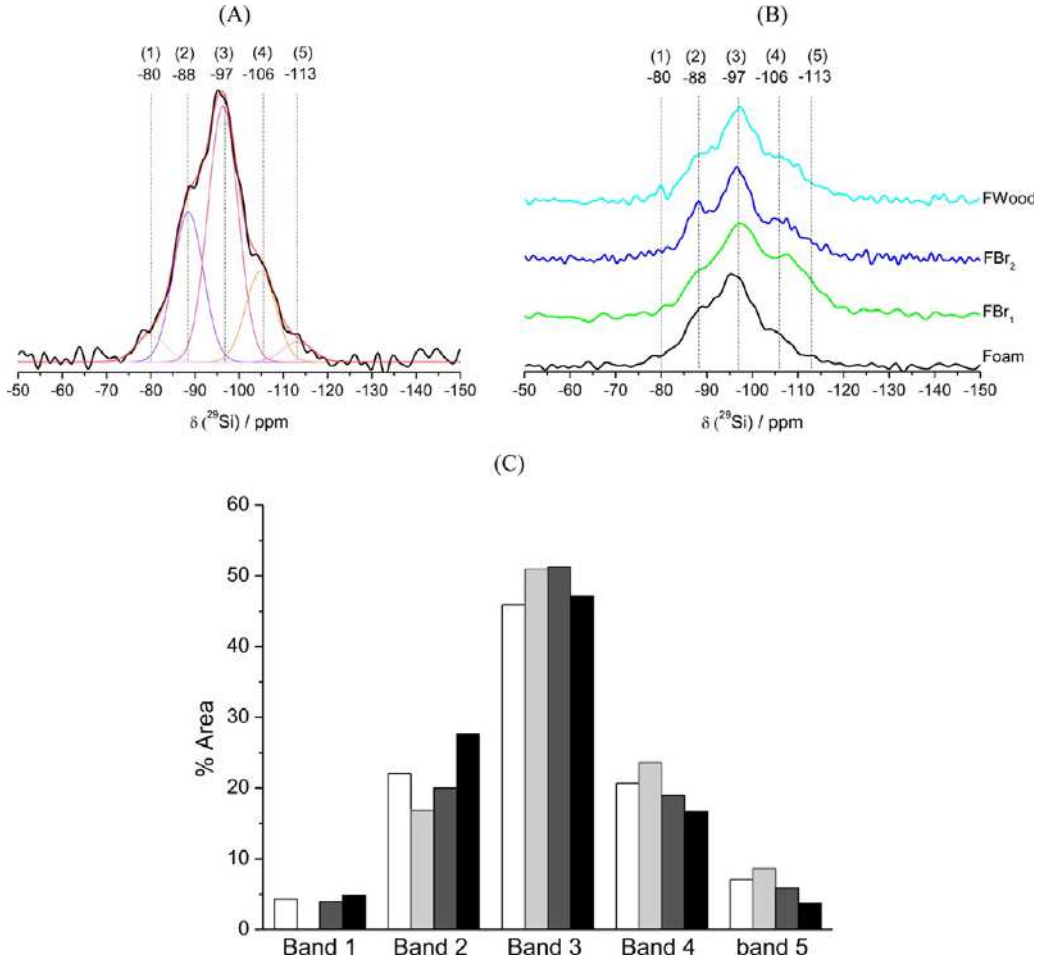

Figure 3. ^{29}Si MAS NMR results: (A) deconvoluted spectra in the case of FDS_{100} (foam); (B) experimental data for FDS_{100}Wood, $FDS_{100}Br_1$, $FDS_{100}Br_2$, and FDS_{100}; and (C) percentage of the area of each contribution determined from deconvulated spectra for (white) FDS_{100}Wood, (light gray) $FDS_{100}Br_1$, (dark gray) $FDS_{100}Br_2$, and (black) FDS_{100}.

dx.doi.org/10.1021/ie403670c | Ind. Eng. Chem. Res. 2014, 53, 3559−3569

Wettability tests were performed by placing a drop of foam FDS_{100} on the wood and bricks at room temperature. Contact angle, absorption, and spreading characteristics were observed.

The BET specific surface area of the silicas was determined by N_2 adsorption at −195.85 °C using a Micrometrics Tristar II 3020 volumetric adsorption/desorption apparatus. Prior to measurement, the samples were degassed at 200 °C under vacuum for 4 h (Supporting Information, Table S1).

RESULTS

Interaction between Materials. To determine if the adhesion between the materials is possible, it is important to obtain data on the wetting properties and materials surface.

Wettability Test. Wettability test results are gathered as Supporting Information (Table S3). Wettability tests on bricks and wood provide information about the drop spreading and underline the different absorption properties of the materials. The wettability tests show that the contact angle at $t = 0$ was closed to 90° for wood and Br_1, while for Br_2 it is below 90°. At $t = 7$ min all angles are below 90°. This result therefore justifies an adhesive compatibility between these materials. The absorption is significantly higher for brick Br_1 than for brick Br_2. After less than 5 min, an aureole was visible around the drop deposited on Br_1, justifying the absorption of part of the binder by the brick. For Br_2, no aureole was observed, which can be explained by a difference in terms of total porosity and pore size distribution of the bricks. The porosity values determined by mercury intrusion of each brick are 35% and 21% for Br_1 and Br_2, respectively.[12] Moreover, the median pore diameter of the Br_1 brick is approximately 3.7 μm, and the pores are mostly between 1 and 10 μm. For the Br_2 brick, the pores are smaller, with a pore size distribution ranging from 0.005 to 0.8 μm and the median diameter at approximately 0.7 μm. Penetration of the binder into the brick depends on the pore size. In the case of the Br_1 brick, the binder can easily penetrate into the large pores, allowing it to penetrate deeper and faster compared to the Br_2 brick. For wood, absorption is intermediate and differs according to its nature, as it is more important for the spring wood than the summer wood.[20] These observations warrant a penetration of binder materials. The low contact angle also reflects an easy adhesion between these materials.

The wettability tests have shown that there was binder penetration through the pores of the material. This observation is corroborated by the mechanical shear and pull-out tests performed in a previous study.[13] The penetration of the binder induces necessary chemical interactions, with materials being able to modify the nature of the networks formed inside the once consolidated binder.

Analysis of Interactions between the Binder and Structural Materials. To highlight and better understand the various interactions occurring at the local scale, nuclear magnetic resonance and FTIR spectroscopic analyses were performed to determine the environments of the silicated species of the binder.

MAS NMR Analysis. The silicated species are described with the usual notation, Q^n, where n ranging between 0 and 4 indicates the degree of connectivity of silicon, i.e., the number of bridging oxygens.[21] The differentiation of the numerous species is obtained by the study of the chemical shift, which strongly depends on the coordination number of silicon. In a geopolymeric binder, the silicon is principally in a tetrahedral coordination and is bonded with aluminum. Thus, for geopolymer materials, the $Q^n(mAl)$ notation is used to describe the environment of silicon, where m ranges from 0 to 4 and represents the number of connected aluminum atoms. As before, n ranging between 0 and 4 indicates the number of bridging oxygens.[22] For example, Autef et al. have put in evidence for a dense geopolymer for which bands centered around −90, −95, −100, −105, and −110 ppm can be attributed to $Q^4(4Al)$, $Q^4(3Al)$, $Q^4(2Al)$, $Q^4(1Al)$, and $Q^4(0Al)$, respectively.[23] Moreover, it has to be noted that in function of the chemical composition the position of the band can be slightly different.[24]

Figure 3A shows the spectrum of the reference binder (foam FDS_{100}) used for the construction of the building system. This spectrum was deconvoluted into five contributions, in accordance with the phases highlighted by the work of Prud'homme et al.[25] on this material: three major contributions centered at −88, −97, and −106 ppm, denoted as contribution 2, 3, and 4, respectively, and two minor contributions centered at −80 and −113 ppm, denoted as contribution 1 and 5, respectively.

Minority phases may be attributed to the contribution of depolymerized species [species $Q^3(1Al)$, Tognonvi et al.[26]] for band 1 (−80 ppm) and silicic acid for band 5 (−113 ppm).[27,28]

Band 2 (−88 ppm), present in the binder, can be attributed to the main contribution of the geopolymer phase.[29] In comparison to the literature on geopolymer materials, the position of the observed chemical shift (band 2) varies slightly. This can be explained by the difference of the reaction medium as a result of the release of dihydrogen and different levels of silica.[13,25] Contribution 4, centered around −106 ppm, can be attributed to quartz[30,31] present in the metakaolin or silicate species of silica gel.[26,16] Finally, contribution 3, the largest band located at −97 ppm, may be attributed to (i) a zeolite phase, (ii) a $K_2Si_2O_5$ phase, or (iii) the presence of siliceous species in $Q^3(2Al)$ corresponding to an environment of an aluminosilicate material.[25,32−36] This contribution will be used for reference later in the study as the primary aluminosilicate compound, but it should be noted that the element potassium is also present.

Figure 3B presents the ^{29}Si MAS NMR spectrum of the reference binder (foam FDS_{100}, Si/K = 2.6, Si/Al = 3.93) and the spectrum of the same binder consolidated in contact with each of the three materials ($FDS_{100}Br_1$, $FDS_{100}Br_2$, and FDS_{100}Wood).

In general, whichever material is in contact with the binder, there is always a prevalence of band 3 centered at −97 ppm (Figure 3B). Other contributions located at −88, −106, and −113 ppm show variable intensities. It should be noted that contribution 1 (−80 ppm) is not detected on the deconvoluted spectrum of the $FDS_{100}Br_1$ sample.

To understand the phenomena responsible for these intensity differences, the integrated area of each contribution for FDS_{100}Wood, $FDS_{100}Br_1$, $FDS_{100}Br_2$, and FDS_{100} (foam) samples was plotted in Figure 3C. This representation allows for the evaluation of the contributions of the different networks present after consolidation. As seen above, contribution 3 is always present and was therefore considered as the main band. This shows that the species within the porous aluminosilicate geopolymer binder are not changed. It should be noted that contribution 2, attributed to the geopolymer phase, decreased for all the samples. This suggests a decrease of aluminosilicate species inside the binder necessary for the formation of the geopolymer network. This fact is more pronounced for the $FDS_{100}Br_1$ sample. In return, this phenomenon is compensated

dx.doi.org/10.1021/ie403670c | Ind. Eng. Chem. Res. 2014, 53, 3559−3569

for by an increase in the contributions of environments 4 and 5 for all the samples, but in different proportions, depending on the substrate in contact with the binder.

(i) In the case of wood support (FDS_{100}Wood), the slight decrease of the geopolymer band (−88 ppm) associated with an increase of the characteristic band of silica gel (−106 ppm) and silicic acid (−113 ppm) is a result of the penetration of the binder into the wood fibers. Indeed, this very hygroscopic support has a high affinity for alkaline aqueous solutions.[37] This is in agreement with the transfer of the potassium element observed in a previous study.[12] The species in interaction with the wood are silicated species enriched with potassium.

(ii) In the case of the $FDS_{100}Br_2$ sample, the low intensity of the contribution of silicic acid (−113 ppm) can be explained by an in-depth limited penetration of the binder. Indeed, this brick composed of small pores (from 0.01 to 0.80 μm) does not allow the species present in the reaction medium to penetrate deeply (<100 μm) into the brick. This fact will locally induce an alteration of the brick by a partial dissolution of clays in the alkaline medium and release species that will be able to react and supply the geopolymer phase whose contribution varies slightly.[38]

(iii) In the case of the $FDS_{100}Br_1$ sample, the binder will also enter the brick but more deeply (>500 μm) as a result of its higher pore size (1−10 μm). In this case, the species released by the deterioration of brick will tend to react locally, consuming the species necessary for the formation of the geopolymer phase in the binder. This will result in the creation of different speciation equilibriums and thus create a chemical interaction in the liquid precursor, thus changing the pH value. Then, there will be a reduction in that value which will promote the appearance of silica gel and silicic acid.[39]

The low contribution at −80 ppm for FDS_{100}Wood and $FDS_{100}Br_2$ characterizes the presence of aluminosilicate depolymerized diluted species.[40] These materials will not be able to condense and participate in the various networks. In the case of the $FDS_{100}Br_1$ sample, with the reaction mixture having diffused into brick, there is little or no formation of these isolated depolymerized species.

The NMR spectroscopy results have evidenced various networks formed after interactions with materials.

In Situ FTIR Analysis. FTIR spectroscopy results on the binder with support tests ($FDS_{100}Br_1$, $FDS_{100}Br_2$ and FDS_{100}Wood) provide information on possible interactions during the consolidation of the binder in contact with the materials. In situ monitoring of samples over a 10-h period gives information about the rearrangement of the network. In particular, the band centered at approximately 980 cm^{-1} shifts to a lower value during the formation, which is characteristic of the geopolymerization reaction and corresponds to the Si−O−M (M = Si or Al) vibration band.[12,18] By monitoring this displacement, it is possible to evaluate the kinetics of the geopolymerization (slope of the curve) and the structural evolution of the network (total displacement of the band). In situ FTIR monitoring tests performed on the reference binder, FDS_{100}Wood, $FDS_{100}Br_1$, and $FDS_{100}Br_2$ show a strong difference in terms of reaction kinetics and formed networks. This result confirms the interactions between the binder and materials during the consolidation. Figure 4 shows the evolution of the position of the band corresponding to the Si−O−M bonds versus time for FDS_{100}, $FDS_{100}Br_1$, $FDS_{100}Br_2$, and FDS_{100}Wood samples. The variations may be divided into two regimes depending on time. At the beginning, for all samples, there is an increase of the displacement value of the band Si−O−M. After approximately 100 min, there is an inversion of variation.

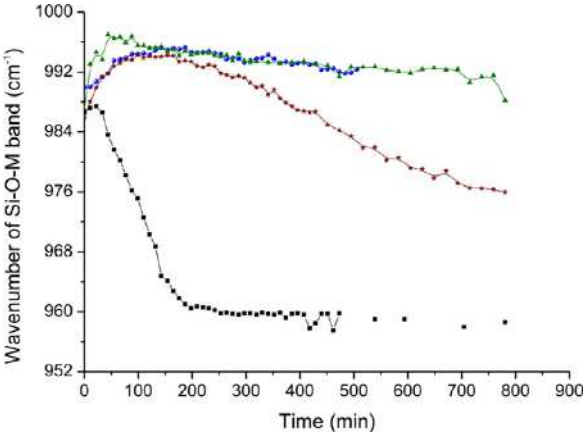

Figure 4. Wavenumber evolution of the Si−O−M band as a function of time for (blue circle) $FDS_{100}Br_1$, (red star) $FDS_{100}Br_2$, (green triangle) FDS_{100}Wood, and (black square) FDS_{100} (foam).

(i) From the first minutes of the reaction ($t < 100$ min), the increase of the position of the Si−O−M band translates to different speciation equilibriums, likely resulting from absorption phenomena by the various supports. This suggests that there is Si−O−Si entities formation as silicic acid is observed by NMR.[26]

(ii) After 100 min, two types of behaviors are observed, one characteristic of geopolymerization reactions with a significant decrease in the Si−O−M band position ($FDS_{100}Br_2$) and the other characteristic of a metastable equilibrium with very little variation of displacement ($FDS_{100}Br_1$ and FDS_{100}Wood). In the case of the $FDS_{100}Br_2$ sample, the existence of interactions between the altered clay particles and the reaction medium can lead to various aluminosilicate networks observed by NMR. For $FDS_{100}Br_1$ and FDS_{100}Wood samples, as a result of greater binder penetration into the support, the speciation equilibriums are modified. This leads to a metastable state that is characterized by few transfers of species. Interactions are limited, and thus, in situ geopolymerization reaction detection is difficult.

These results are in agreement with the wettability tests presented previously, which show that the absorption time of a drop of binder is more important for Br_1 brick than for wood and the Br_2 brick.

Effect of Siliceous Species on the Binder Formulation Mechanism. Differences were observed between the binder alone and the binder in contact. The differences were explained by a variation of the availability of the siliceous species. It then appears judicious to understand the role of certain siliceous species in speciation equilibriums by modifying the amount of silica introduced. New formulations denoted "variation" and "substitution" were tested, where the nature and the amount of silica introduced were the parameters of study. In this case, each binder was consolidated under the environmental conditions without support contact. Six different sets of formulations were synthesized and analyzed by in situ FTIR.

Description of Substitution and Variation Tests. For each formulation of each set, the monitoring of the Si−O−M band was performed and the total displacement and slope of the curve were measured and compared. Parts A and B of Figure 5

dx.doi.org/10.1021/ie403670c | Ind. Eng. Chem. Res. 2014, 53, 3559−3569

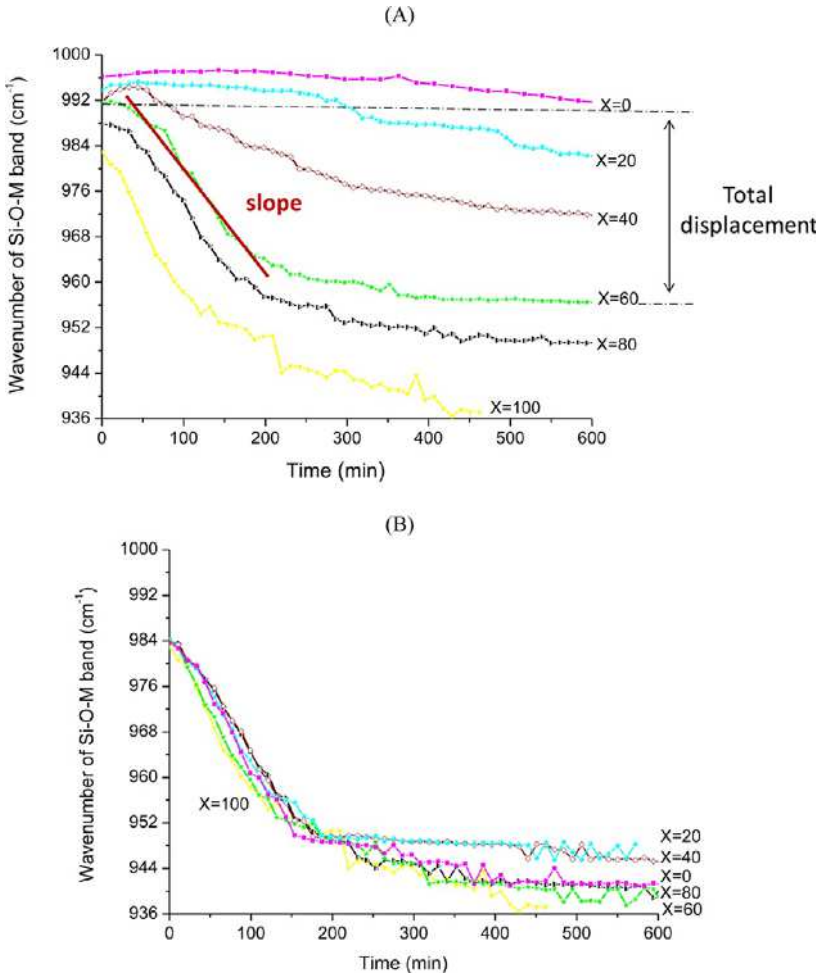

Figure 5. Evolution of Si−O−M band position in function of time for (A) $Si400_XM5_{100-X}$ and (B) $Si400_X$ series.

present the evolution of the Si−O−M band position as a function of time for the series substitution $Si400_XM5_{100-X}$ and variation $Si400_X$, respectively. Moreover, a picture of all samples synthesized was taken after 1 week of drying at ambient temperature and are gathered as Supporting Information (Table S4). It is observed that as a function of type and amount of silica added, the morphology of the samples differ. Subsequently, both the features of the samples synthesized as well as the monitoring of the Si−O−M band will be discussed.

FDS_XSi400_{100-X}. The FDS_0Si400_{100}, $FDS_{20}Si400_{80}$, and $FDS_{40}Si400_{60}$ samples show two distinct phases after consolidation: one having the appearance of a dense geopolymer without cracking (lower phase) and the other being glassy, similar to a silica gel (top). The other formulations ($FDS_{60}Si400_{40}$ and $FDS_{80}Si400_{20}$) have a uniform appearance but with shrinkage on the bottom and an upper portion resembling a gel. Both types of behavior are primarily because of the FDS/Si400 ratio that imposes the rate of silicon available, which goes into solution and participates in the reaction. Regardless of the sample type, there is a decrease of the displacement value, which characterizes the polycondensation reactions between the different aluminosilicate species. However, the more silica Si400 increases, the more the overall value of the displacement quickly increases. This result can be explained by the following parameters.

(i) When X = 0, a reagent mixture between the metakaolin and the alkaline solution is created, which leads to the geopolymer network formation. Excess species that do not react contribute to the development of a gel on the surface. Si400 particles are encapsulated in the geopolymer binder.

(ii) When 0 < X < 60, competition between different networks (geopolymer and gel) exists by the interaction of silica fume FDS, which generates dihydrogen and releases siliceous species that can participate in geopolymeric networks.

(iii) When X 60, a very high reactivity of the silica fume FDS is observed, which controls the reactivity of the medium by releasing siliceous species.

FDS_XM5_{100-X}. All samples in this series exhibit one phase, except for the biphasic $FDS_{20}M5_{80}$. A difference of volume expansion is observed in these samples, which is more important than the high amount of FDS silica.[41] The shift of the Si−O−M band decreases when the proportion of M5 silica fume increases. The difference in reactivity of the two silicas is directly related to their specific surface area, 40 and 202 m^2/g for FDS and M5, respectively. In the presence of a significant amount of M5, after several minutes, the medium becomes saturated with siliceous species. Then, there is competition between the formation of a Si-rich network and geopolymerization reactions, which are characterized by a very low shift of the Si−O−M band. This observation is

dx.doi.org/10.1021/ie403670c | Ind. Eng. Chem. Res. 2014, 53, 3559−3569

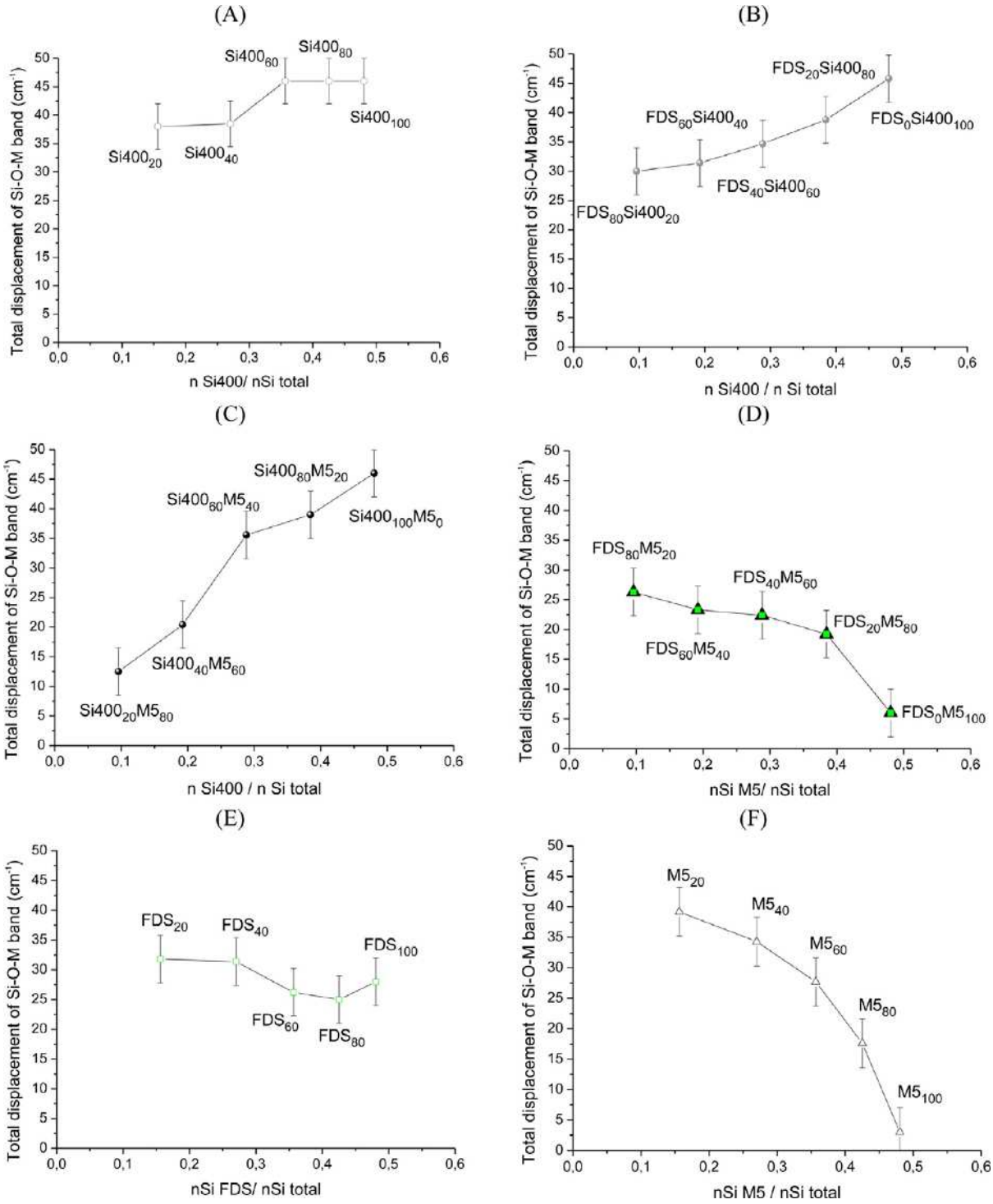

Figure 6. FTIR total displacement variation value according to the (nSi introduced)/(nSi total) ratio for (A) $Si400_X$, (B) FDS_XSi400_{100-X}, (C) $Si400_XM5_{100-X}$, (D) FDS_XM5_{100-X}, (E) FDS_X, and (F) $M5_X$.

corroborated by the slope of the curve near zero for $M5_{100}$, characteristic of a saturated siliceous medium and by its increase with the augmentation of the amount of FDS silica.

$Si400_XM5_{100-X}$ Series. Two distinct types of behavior and an intermediate behavior are observed. For $X < 40$, the mixture appears homogeneous, but evolves with time. Next, there appears a central collapse, suggesting that some species have precipitated.[39] For $X \approx 40$, two phases appear; the lower portion resembles a dense geopolymer, while the upper portion exhibits a glassy aspect. Moreover, the volume of the upper phase increases with the increase of Si400 silica. Regardless of the sample, the more the M5 quantity increases, the greater the shift of the Si−O−M band and the slope decreases. As for the FDS_XSi400_{100-X} substitution, the low-reactive silica Si400

dx.doi.org/10.1021/ie403670c | Ind. Eng. Chem. Res. 2014, 53, 3559−3569

(crushed quartz) has little influence on the formation of the network and the viscosity. This difference in reactivity is directly related to their specific surface area, 1 and 202 m^2/g for Si400 and M5, respectively.

FDS_X series. Two types of consolidation are observed. For $X < 60$, there are two separate phases; the lower portion has a dense geopolymer appearance without cracking, while the upper phase shows a glassy feature with a porous interface. For $X \geq 60$, samples after consolidation show heterogeneities because of the release of H_2 gas and the amount of siliceous species in the reactive medium. These species are the origin of the formation of various phases. The variation in the amount of FDS silica fume certainly causes a different distribution of observed phase within the geopolymer foam, i.e., silica gel, $K_2Si_2O_5$ compound, zeolite, and the geopolymer network.[25] The value of the shift of the Si−O−M band decreases with the augmentation of the amount of FDS silica fume. FDS_{20}/FDS_{40} and FDS_{60}/FDS_{80} show nearly identical final displacement values of approximately 32 and 26 cm^{-1}, respectively. These variations are in agreement with the zones identified previously (specifically for $X < 60$, a higher value of displacement, and for $X \geq 60$, a lower value) and with the work of Prud'homme et al.[25] Indeed, the reduction of FDS silica fume will promote the formation of a geopolymer network, and its formation will be more significant than the high displacement value. For low levels of silica, the composition approaches a single geopolymer network. In contrast, when the amount of FDS silica fume increases, there is competition between the formation of different compounds, such as silica gel, $K_2Si_2O_5$ compound, the zeolite phase, and the geopolymer network.

$M5_X$ Series. As before, the $M5_X$ series shows two types of behavior. For $X \geq 60$, a single phase is obtained, which has the appearance of a gel that will eventually collapse. For $X < 60$, two phases appear; the lower portion resembles a dense geopolymer, while the upper phase exhibits a glassy aspect. As previously described, the increase in available silica causes a decrease in displacement as a result of the competition between the different aluminosilicate species. When the amount of silica is sufficient to form a network geopolymer, it forms very quickly ($0 < X < 40$). In the opposite case ($X \geq 40$), there is again a competition between a geopolymer network and a saturated siliceous species liquid, which leads to a gel. These phenomena are also observable by the variation in slopes.

$Si400_X$ Series. Finally, for the $Si400_X$ series, two phases can be distinguished for all the samples. The bottom phase has features of a dense geopolymer, whereas the upper phase shows a vitreous aspect and presents a great deal of shrinkage, and their interface shows cracking. The augmentation of the amount of Si400 silica has no influence on the Si−O−M band shift value, which remained approximately 40 cm^{-1} for all samples. This highlights the very low reactivity of Si400 in the reaction medium. In this case, the Si400 silica simply plays the role of reinforcement.[42] Nevertheless, the observed demixing (geopolymer phase and gel upon the surface) suggests that the consolidated sample is composed of at least two networks, in accordance with the work of Autef et al.[43]

Summary of the Reactivity and the Nature of the Networks Formed. To compare the different formulations, Figure 6 shows the displacement value of the Si−O−M band determined by FTIR spectroscopy as a function of the ratio of the number of moles of silica (Si400, M5, or FDS) added by the total number of silica in the formulation.

Si400 Influence. The low shift of the band from 38 to 46 cm^{-1} for samples $Si400_{20}$ to $Si400_{100}$ (Figure 6A) as a function of the nSi400/nSi total ratio is characteristic of both the formation of a geopolymer network and the coating of the quartz grain by an aluminosilicate binder.

In the presence of reactive silica, increasing the nSi400/nSi total ratio causes an increase in the displacement value from 29 to 46 cm^{-1} for samples $FDS_{80}Si400_{20}$ to FDS_0Si400_{100} (Figure 6B) and from 12 to 46 cm^{-1} for samples $Si400_{20}M5_{80}$ to $Si400_{100}M5_0$ (Figure 6C). This characterizes the nonreactivity of Si400 silica within the reaction medium because there is little or no release of siliceous species. Nevertheless, the variations are not identical with those of the FDS or M5 silicas. The differences observed reflect their reactivity, which is a function of their ability to release siliceous species in the reaction medium, thus modifying the speciation equilibriums.

FDS and M5 Silica. This reactivity was confirmed during the formation of the FDS_XM5_{100-X} series. The change of the nSiM5/nSi total ratio results in a slight change in the displacement value from 26 to 19 cm^{-1} for samples $FDS_{80}M5_{20}$ to $FDS_{20}M5_{80}$ (Figure 6D). The substitution of FDS by M5 silica leads to modifications in the speciation equilibriums, thus promoting the formation of a silica gel to the detriment of the other networks.

These features are again highlighted for the variation series FDS_X (Figure 6E) and $M5_X$ (Figure 6F). A slight decrease in the shift from 32 to 28 cm^{-1} for FDS_{20} to FDS_{100} and a sharp decrease of the displacement from 39 to 6 cm^{-1} for samples $M5_{20}$ to $M5_{100}$ are noted. Consequently, unlike the FDS silica, with the more reactive M5 silica, the siliceous species are available more quickly to form a gel and therefore decrease the value of displacement.

Global Reactivity. To exacerbate the reactivity of the siliceous species, the displacement of the Si−O−M band as a function of the slope for all the samples was plotted in Figure 7. Three areas can be defined with values of the slope around −0.18 and −0.10 $cm^{-1}\ s^{-1}$. Above −0.10 $cm^{-1}\ s^{-1}$, supersaturated siliceous species will form a Si-rich aluminosilicate gel, whereas below this value, there will be formation of different

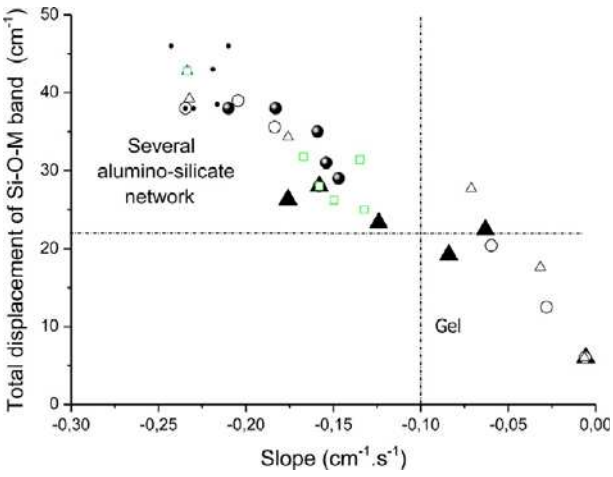

Figure 7. Evolution of the total displacement value versus the FTIR displacement slope value of Si−O−M band position for (filled triangle) FDS_XM5_{100-X}, (open circle) $Si400_XM5_{100-X}$, (large filled circle) $Si400_XFDS_{100-X}$, (open triangle) $M5_X$, (green box) FDS_X, and (small filled circle) $Si400_X$ series.

dx.doi.org/10.1021/ie403670c | Ind. Eng. Chem. Res. 2014, 53, 3559−3569

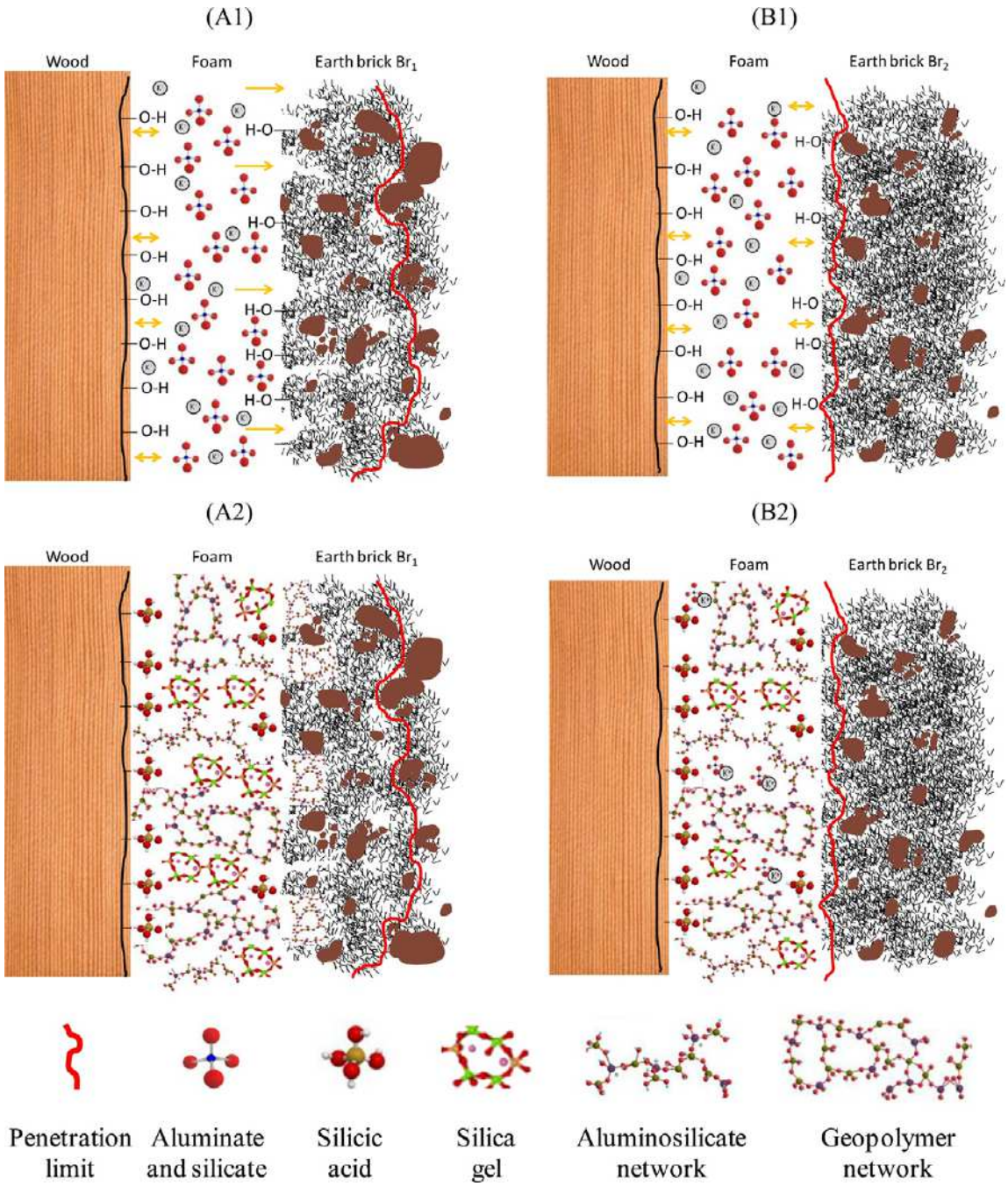

Figure 8. Formation scheme of FDS_{100} (foam) in interaction with wood and brick Br_1 (A) and Br_2 (B) at the beginning (A1, B1) and at the end of the reaction (A2, B2).

aluminosilicate networks. This corresponds to a value of displacement ranging between 0 and 22 cm^{-1}. This observation is corroborated by the work of Gao et al.,[19] which shows that for a value of displacement ranging between 0 and 22 cm^{-1}, there is preferential bridging between the siliceous species, whereas for values higher than 22 cm^{-1}, there is formation of various networks. Moreover, the position of synthesized compounds on the ternary Si−Al−K−O (Figure 2) shows that the different considered formulations are located in the areas of materials leading to gels or sedimented materials presenting several phases. This is in perfect agreement with the results obtained. Moreover, it can define porous materials as the samples presenting a value of slope ranging between −0.18 and −0.10 $cm^{-1}\ s^{-1}$.

From these data, it is thus possible to delimit the existence of various types of materials according to the displacement of the Si−O−M band and the slope of the curve. For a given silicate solution, three areas have been identified: an area corresponding to a Si-rich aluminosilicate gel, an area composed of different porous networks, and an area composed of different dense networks. Moreover, all previous analyses, performed at

dx.doi.org/10.1021/ie403670c | Ind. Eng. Chem. Res. 2014, 53, 3559−3569

constant water content, suggest that it would be possible to move from one area to another by changing the water amount.

DISCUSSION

The previous study helped highlight the different environments present in the binder after contact with the structural materials (earth brick and wood), as well as an existence range of several types of materials by FTIR spectroscopic analysis. In fact, the existence of different networks, especially during the FDS_xM5_{100-x} substitution series, has been shown. From all of these data, the binder formation scheme is proposed for the two types of assembly in Figure 8. Figure 8 puts forth the various hypotheses on the interaction between materials explained below. For the two types of assemblies, the wood and the brick are represented. The evolution of species within the binder is given for different times during the consolidation. It should be noted that there is a scale factor between the representation of wood, brick, and species. For each time, the different contributions and the different networks described above were reported.

Interaction of Wood/Binder. Morphological (wettability) and structural (NMR and FTIR) analyses have shown the absorption of the binder by wood porosity. Moreover, it has been shown that after consolidation, the Si-rich aluminosilicate network and silica gel were still present. The geopolymer phase is also present but in smaller quantities. The decrease in geopolymer phase suggests that there has been a decrease in siliceous species able to react with the aluminous species. This defect of concentration in siliceous species may be characteristic of an exchange with the wood.

Consequently, at the time of the contact with wood, as shown in Figure 8 (A1 and B1), the exchange highlighted in previous work[12] is thus ensured by the potassium silicate solution. This gives the local formation of silicic acid (band at −113 ppm). This type of acid can be formed with a reduction of pH value, which can occur during the transfer of the mixture within the wood fibers, wood being acidic in nature.[44] This phenomenon will result in the creation of siliceous depolymerized species richer in aluminum (band at −80 ppm). These data corroborate the observations by FTIR spectroscopy, initiated by an exchange of siliceous species in supersaturation (formation of silicic acid justified by the increase of the Si−O−M band position), followed by the depolymerized species (light shift of the band position).[43]

Interaction of Br_2/Binder. In the same manner, the morphological and structural analyses showed a slow and diffuse absorption of the binder by the Br_2, which is characterized by a small pore size. The same contributions, i.e., a geopolymer network, a Si-rich aluminosilicate environment, and silica gel, are noted. The siliceous species in solution, in the presence of the surface of brick, will interact and form simultaneously (i) the silicic acid from the penetration of the binder and (ii) a geopolymer phase because of the local attack of the clay particles. The formation of depolymerized species also suggests that an excess of siliceous species (in very small amount) does not participate in the network formation (low intensity at −80 ppm). In addition, FTIR spectroscopy reflects the solvent absorption with the creation of silicic acid as before, as shown in Figure 8B1. Then, there is the formation of different networks justified by the large displacement of the Si−O−M band, as show in Figure 8B2.

The presence of these depolymerized species and of silicic acid can certainly promote interactions and enhance adhesion between materials.

Interaction of Br_1/Binder. In this case, the morphological (visual and wettability tests) and structural (NMR and FTIR) analyses showed very strong absorption of the binder by the brick Br_1 because of its large pore sizes. The major identified networks are the geopolymer, the Si-rich aluminosilicate compound, and the silica gel with the largest contribution. Again, upon contact with the brick surface, there is formation of silicic acid, followed by a quick diffusion through the material. This creates locally, in small amounts, the geopolymer networks and thus increases the formation of silica gel. The absence of the band at −80 ppm (depolymerized species) can be explained by the reactions in the brick that consume all available species. FTIR analysis confirms the various interactions leading to the different networks.

CONCLUSION

This study was focused both to describe and to understand the phenomena that occur between a geopolymer binder and structural materials, such as mud brick and wood, and also to identify the effect of siliceous species on the binder consolidation.

Various formulations containing different silicas were used to establish the areas of compositions, which result in either a homogeneous material or different types of networks, depending on the reactivity of silica introduced. All of these results, associated with NMR (^{29}Si) and FTIR analyses, allowed for the complete understanding of transfers that occur at the interfaces. The different network contributions highlighted in the porous geopolymer binder (FDS_{100}) were modified during the consolidation and depend on the interactions with the brick and the wood. In particular, different proportions of the geopolymer phase were observed as a result of the contact with the bricks and the formation of silicic acid in the majority resulting from the contact with wood. Moreover, these data are closely related to the amount and nature of siliceous species available in solution that govern the nature of the monomers and the formation kinetics.

Additionally, to complement previous studies and validate the feasibility of such building system, a full scale ($2 \times 2\ m^2$) wall was built, and various tests in a climate chamber were performed to investigate the hygrothermal regulation efficiency.

ASSOCIATED CONTENT

* Supporting Information

Tables S1−S4, as noted in the text. This material is available free of charge via the Internet at http://pubs.acs.org.

AUTHOR INFORMATION

Corresponding Author

*E-mail: sylvie.rossignol@unilim.fr. Tel.: +33 5 87 50 25 64.

Notes

The authors declare no competing financial interest.

ACKNOWLEDGMENTS

We thank Isabelle Sobrado and Jesus Sanz from Instituto de Ciencia de Materiales de Madrid, Consejo Superior de Investigaciones Cientificas (CSIC), Madrid, Spain.

REFERENCES

(1) McLellan, B. C.; Williams, R. P.; Lay, J.; Van Riessen, A.; Corder, G. D. Costs and carbon emissions for geopolymer pastes in comparison to ordinary portland cement. J. Cleaner Prod. 2011, 19, 1080−1090.

(2) Venkatarama Reddy, B. V.; Jagadish, K. S. Embodied energy of common and alternative building materials and technologies. Energy Build. 2003, 35, 129−137.

(3) Duxson, P.; Provis, J. L.; Lukey, G. C.; Van Deventer, J. S. J. The role of inorganic polymer technology in the development of 'green concrete'. Cem. Concr. Res. 2007, 37, 1590−1597.

(4) Minke, G. Building with Earth, 2nd ed; Birkhauser: Basel, 2006.

(5) Houben, H.; Guillaud, H. Traite de Construction en Terre, 3rd ed; Parentheses: Marseille, 2006.

(6) Fontaine, L.; Anger, R. Batir en Terre, 1st ed.; Belin: Paris, 2010.

(7) Morton, T. Earth Masonry: Design and Construction Guidelines, 1st ed.; BRE Press: Bracnell, 2008.

(8) Morel, J.; Mesbah, A.; Oggero, M.; Walker, P. Building houses with local materials: Means to drastically reduce the environmental impact of construction. Build. Environ. 2001, 36, 1119−1126.

(9) Allinson, D.; Hall, M. Hygrothermal analysis of a stabilised rammed earth test building in the UK. Energy Build. 2010, 42, 845−852.

(10) Lawrence, M.; Heath, A. C.; Walker, P. Development of a Novel Binder for Mortar for Unfired Clay Bricks. Proceeding of Second International Conference on Sustainable Construction Materials and Technologies; Ancona, Italy, June 28−30, 2010.

(11) Prud'Homme, E.; Michaud, P.; Joussein, E.; Peyratout, C.; Smith, A.; Sauvat, N. et al. Geomaterial foam to reinforce wood. Proceeding of the 34th International Conference on Advanced Ceramics and Composites; Daytona Beach, FL, January 24−29, 2010.

(12) Gouny, F.; Fouchal, F.; Maillard, P.; Rossignol, S. A geopolymer mortar for wood and earth structure. Constr. Build. Mater. 2012, 36, 188−195.

(13) Gouny, F.; Fouchal, F.; Pop, O.; Maillard, P.; Rossignol, S. Mechanical behavior of an assembly of wood−geopolymer−earth bricks. Constr. Build. Mater. 2013, 38, 110−118.

(14) Davidovits, J. Chemistry and Applications; Institut Geopolymere: Saint Quentin, 2008.

(15) Xu, H. Geopolymerisation of aluminosilicate minerals. PhD. Thesis, University of Melbourne, 2001.

(16) Autef, A.; Joussein, E.; Poulesquen, A.; Gasgnier, G.; Pronier, S.; Sobrados, I.; Sanz, J.; Rossignol, S. Influence of metakaolin purities on potassium geopolymer formulation: The existence of several networks. J. Colloid Interface Sci. 2013, 408, 43−53.

(17) Prud'Homme, E.; Michaud, P.; Joussein, E.; Clacens, J. M.; Rossignol, S. Role of alkaline cations and water content on geomaterial foams: Monitoring during formation. J. Non-Cryst. Solids 2011, 357, 1270−1278.

(18) Lee, W. K. W.; Van Deventer, J. S. J. Use of infrared spectroscopy to study geopolymerization of heterogeneous amorphous aluminosilicates. Langmuir 2003, 19, 8726−8734.

(19) Gao, X. X.; Autef, A.; Prud'homme, E.; Michaud, P.; Joussein, E.; Rossignol, S. Synthesis of consolidated materials from alkaline solutions and metakaolin: Existence of domains in the Al-Si-K/O ternary diagram. J. Sol-Gel Sci. Technol. 2012, 65, 220−229.

(20) Benoit, Y. Le Guide des Essences de Bois, 2nd ed.; Eyrolle: Paris, 2008.

(21) Engelhardt, G.; Zeigan, D.; Jancke, H.; Hoebbel, D.; Wieker, W. ^{29}Si NMR spectroscopy of silicate solutions. II. On the dependence of structure of silicate anions in water solutions from the Na/Si ratio. Z. Anorg. Allg. Chem. 1975, 418, 17−28.

(22) Engelhardt, G.; Lohse, U.; Samoson, A.; Magi, M.; Tarmak, M.; Lippmaa, E. High resolution ^{29}Si NMR of dealuminated and ultrastable Y-zeolites. Zeolites 1982, 2, 59−62.

(23) Rossignol, S.; Prud'Homme, E.; Michaud, P.; Joussein, E.; Sobrado, I.; Sanz, J. Reply to the J. Provis and S.A. Bernal comment about the article "Structural characterization of geomaterial foams. Thermal behavior". J. Non-Cryst. Solids. 2012, 358, 717−718.

(24) Autef, A. Formulation geopolymere: Influence des rapports molaires Si/K et Si/Al sur les reactions de polycondensation au sein de gels aluminosilicates. PhD. Thesis, University of Limoges, 2013.

(25) Prud'Homme, E. Role du cation alcalin et des renforts mineraux et vegetaux sur les mecanismes de formation de geopolymeres poreux ou denses. PhD. Thesis, University of Limoges, 2011.

(26) Tognonvi, M. T.; Massiot, D.; Lecomte, A.; Rossignol, S.; Bonnet, J-P. Identification of solvated species present in concentrated and dilute sodium silicate solutions by combined ^{29}Si NMR and SAXS studies. J. Colloid Interface Sci. 2010, 352, 309−315.

(27) Chemtob, S. M.; Rossman, G. R.; Stebbins, J. F. Natural hydrous amorphous silica: Quantitation of network speciation and hydroxyl content by ^{29}Si MAS NMR and vibrational spectroscopy. Am. Mineral. 2012, 97, 203−211.

(28) Spinde, K.; Pachis, K.; Antonakaki, I.; Paasch, S.; Brunner, E.; Demadis, K. D. Influence of polyamines and related macromolecules on silicic acid polycondensation: Relevance to "soluble silicon pools"? Chem. Mater. 2011, 23, 4676−4687.

(29) Duxson, P.; Provis, J. L.; Lukey, G. C.; Separovic, F.; Van Deventer, J. S. J. ^{29}Si NMR study of structural ordering in aluminosilicate geopolymer gels. Langmuir 2005, 21, 3028−3036.

(30) Zibouche, F.; Kerdjoudj, H.; d'Espinose de Lacaillerie, J-B.; Van Damme, H. Geopolymers from Algerian metakaolin. Influence of secondary minerals. Appl. Clay Sci. 2009, 43, 453−458.

(31) Thompson, J. G. ^{29}Si and ^{27}Al nuclear magnetic resonance spectroscopy of 2:1 clay minerals. Clay Miner. 1984, 19, 229−236.

(32) Dove, M. T. The use of ^{29}Si MAS-NMR and Monte Carlo methods in the study of Al/Si ordering in silicates. Geoderma 1997, 80, 353−368.

(33) Sen, S.; Youngman, R. E. NMR study of Q-speciation and connectivity in K_2O-SiO_2 glasses with high silica content. J. Non-Cryst. Solids 2003, 331, 100−107.

(34) Meneau, F.; Neville Greaves, G.; Winter, R.; Vaills, Y.; WAXS, N. M. R. studies of intermediate and short range order in K_2O-SiO_2 glasses. J. Non-Cryst. Solids 2001, 293, 693−699.

(35) De Jong, B.; Super, H. T. J.; Spek, A. L.; Veldman, N.; Nachtegaal, G.; Fischer, J. C. Mixed alkali systems: Structure and ^{29}Si MAS NMR of $Li_2Si_2O_5$ and $K_2Si_2O_5$. Acta Crystallogr. Sect. B: Struct. Sci. 1998, 54, 568−577.

(36) Todea, M.; Turcu, R. V. F.; Frentiu, B.; Tamasan, M.; Mocuta, H.; Ponta, O.; Simon, S. Amorphous and nanostructured silica and aluminosilicate spray-dried microspheres. J. Mol. Struct. 2011, 1000, 62−68.

(37) Pereyra, A. M.; Giudice, C. A. Flame-retardant impregnants for woods based on alkaline silicates. Fire Saf. J. 2009, 44, 497−503.

(38) Bauer, A.; Berger, G. Kaolinite and smectite dissolution rate in high molar KOH solutions at 35 and 80 °C. Appl. Geochem. 1998, 13, 905−916.

(39) Tognonvi, M. T.; Rossignol, S.; Bonnet, J-P. Physical-chemistry of sodium silicate gelation in an alkaline medium. J. Sol-Gel Sci. Technol. 2011, 58, 625−635.

(40) Singh, P. S.; Bastow, T.; Trigg, M. Structural studies of geopolymers by ^{29}Si and ^{27}Al MAS-NMR. J. Mater. Sci. 2005, 40, 3951−3961.

(41) Prud'homme, E.; Michaud, P.; Joussein, E.; Peyratout, C.; Smith, A.; Arnii-Clacens, S.; Clacens, J.M.; Rossignol, S. Silica fume as porogent agent in geo-materials at low temperature. J. Eur. Ceram. Soc. 2010, 30, 1641−1648.

(42) Autef, A.; Joussein, E.; Gasgnier, G.; Rossignol, S. Role of the silica source on the geopolymerization rate. J. Non-Cryst. Solids. 2012, 358, 2886−2893.

(43) Autef, A.; Prud'Homme, E.; Joussein, E.; Gasgnier, G.; Pronier, S.; Rossignol, S. Evidence of a gel in geopolymer compounds from pure metakaolin. J. Sol-Gel Sci Technol. 2013, 67, 534−544.

(44) Rowell, R. M. Handbook of Wood Chemistry and Wood Composite, 2nd ed; CRC Press: Boca Raton, FL, 2012.